

1 **Dynamic and Thermodynamic Processes Related to Sea-Ice Surface**  
2 **Melt Advance in the Laptev Sea and East Siberian Sea**

3  
4 Hongjie LIANG,<sup>1</sup> Wen ZHOU<sup>1,2</sup>

5 <sup>1</sup> *Department of Atmospheric and Oceanic Sciences & Institute of Atmospheric Sciences, Fudan*  
6 *University, Shanghai, China*

7 <sup>2</sup> *Center for Polar Ice & Snow and Climate Change Research, Polar Research Institute of China,*  
8 *Shanghai, China*

9  
10  
11 *Correspondence to: Wen Zhou (wen\_zhou@fudan.edu.cn)*

12  
13  
14  
15 *Aug, 2023*  
16

17 ABSTRACT

18 Arctic summer sea ice has shrunk considerably in recent decades. This study  
19 investigates springtime sea-ice surface melt onset in the Laptev Sea and East Siberian  
20 Sea, which are key seas along the Northeast Passage. Instead of region-mean melt onset,  
21 we define an index of Melt Advance, which is the areal percentage of a sea that has  
22 experienced sea-ice surface melting before the end of May. Four representative  
23 scenarios of Melt Advance in the region are identified. Each scenario is accompanied  
24 by a combination of distinct patterns between atmospheric circulation, atmospheric  
25 thermodynamic state, sea ice cover (polynya activity), and surface energy balance in  
26 May. In general, concurrent with faster Melt Advance are warmer and wetter  
27 atmosphere, less sea ice cover, and surface energy gains in spring. Melt Advance can  
28 be potentially used in the practical seasonal prediction of, ~~like sea ice cover in May, is~~  
29 ~~significantly correlated with~~ summer sea ice cover. This study implicates the  
30 interannual and interdecadal flexibility of spring circulation in the lower troposphere  
31 and the significance of seasonal evolution in the Arctic.

32  
33  
34 **1. Introduction**

35 Since the 1970s, satellites have enabled global detection of the Earth. Arctic  
36 summer sea ice extent is found to have decreased dramatically in the past four decades  
37 (Petty et al., 2020; Stroeve and Notz, 2018), which is a prominent indicator of global  
38 warming. In fact, the Arctic has a faster warming trend than elsewhere on the planet,  
39 especially in the lower troposphere during the cold season (Cohen et al., 2014; Serreze  
40 et al., 2009; Screen and Simmonds, 2010). This phenomenon, called Arctic  
41 Amplification, presumably results from reduced sea ice cover and enhanced oceanic  
42 energy release toward the atmosphere, atmospheric and oceanic heat transport from  
43 lower latitudes, and local positive feedbacks (Serreze et al., 2009; Cohen et al., 2014;  
44 Taylor et al., 2022). Some research has indicated that the mid-latitudes may frequently

45 experience severe winters due to the Arctic Amplification which reduces the meridional  
46 temperature gradient and in turn amplifies the planetary Rossby wave and makes it  
47 more stationary (Francis and Vavrus, 2015). In the Arctic, positive ice-albedo feedback  
48 is active in the melt season (Budyko, 1969; Kashiwase et al., 2017; Sellers, 1969): after  
49 sea ice begins to melt in spring, surface albedo decreases substantially, which favors  
50 more solar radiation absorption and promotes further sea ice melting. Based on this  
51 notion, some studies have tried to predict Arctic summer sea ice cover by sea-ice surface  
52 Melt Onset (MO) in spring, i.e., the date when the sea ice surface begins to form liquid  
53 water (Petty et al., 2017; Wang et al., 2011). Currently, satellite remote sensing helps  
54 us construct the pan-Arctic sea ice MO, which is not possible with only in-situ field  
55 observations. However, for sea ice lateral and bottom melting, satellites are less useful  
56 and buoys are widely employed (Lei et al., 2022).

57 Many studies have touched on sea ice MO in springtime (Drobot and Anderson,  
58 2001; Bliss and Anderson, 2014; Horvath et al., 2021; Crawford et al., 2018; Markus et  
59 al., 2009; Stroeve et al., 2014). Generally, sea ice MO is becoming earlier in most parts  
60 of the Arctic, which is consistent with the Arctic warming. Another notable feature of  
61 MO is its regionality. For example, the Barents Sea, Kara Sea, Laptev Sea, and East  
62 Siberian Sea are around the same latitudes along the Siberian coast, but the MO trends  
63 were -7.1, -5.2, -2.8, and -1.8 days per decade from 1979 to 2013, respectively (Stroeve  
64 et al., 2014). Liang and Su (2021) investigated the interannual early/late relationship of  
65 MO between the Laptev Sea and East Siberian Sea, which is related to the large-scale  
66 atmospheric pattern of the Barents Oscillation (Skeie, 2000). Locally, synoptic  
67 processes are regarded as responsible for interannual variability. Mortin et al. (2016)  
68 argued that sea ice MO is generally associated with higher surface air temperature  
69 (SAT), total-column water vapor (TWV), and cloud cover, which promotes downward  
70 longwave radiation.

71 The Laptev Sea (LS) and East Siberian Sea (ESS) are marginal seas of the Arctic  
72 Ocean, north of Siberia along the Northeast Passage (Fig. S1). The longitude-latitude

73 ranges are around 70°N-80°N and 100°E-180°, covering 0.66 and 1.14 million km<sup>2</sup> for  
74 the LS and ESS, respectively. These two seas are among the regions where sea ice  
75 decline in September during the past four decades has been the most prominent, and  
76 they are key regions for safe transportation across the Northeast Passage. In spring, sea  
77 ice almost completely covers the seas, while in summer, sea ice substantially retreats  
78 off the coast.

79 Focusing on the LS and ESS, which usually have the most persistent sea ice  
80 coverage in the Northeast Passage, this study aims to demonstrate the springtime  
81 processes related to different Melt Advance scenarios and explore the linkage between  
82 springtime Melt Advance and summertime sea ice coverage.

83  
84

## 85 **2. Data and Methods**

86 Sea ice Melt Onset (MO) is the date when the sea ice surface begins to melt in  
87 spring, which is retrieved from satellite passive microwave signals (Markus et al., 2009).  
88 Liquid water has greater emissivity than ice/snow, so surface melting invokes changes  
89 in passive microwave signals. The dataset is distributed by the National Aeronautics  
90 and Space Administration (NASA) Cryospheric Sciences Research Portal. We use the  
91 yearly MO from 1979 to 2018, with a spatial resolution of ~25 km. Following the  
92 method in Liang and Su (2021), we fill in the missing MO values based on surface air  
93 temperature (SAT) datasets from the International Arctic Buoy Programme/Polar  
94 Exchange at the Sea Surface (IABP/POLES) for 1979-2004 and the Atmospheric  
95 InfraRed Sounder (AIRS) for 2005-2018. Although the missing values are not quite a  
96 lot, the analysis here is more convenient if the whole research area in the LS and ESS  
97 is covered.

98 The sea ice concentration (SIC) dataset, called Ocean and Sea Ice Satellite  
99 Application Facility (OSI SAF), is from the European Organization for the Exploitation  
100 of Meteorological Satellites (EUMETSAT) (Lavergne et al., 2019). We use the monthly

101 SIC in May from 1979 to 2018, with a resolution of 25 km. We also examine SIC dataset  
102 by the NASA Team algorithm(Cavalieri et al., 1996), which shows basically the same  
103 patterns in May as OSI SAF.

104 The atmospheric variables and surface energy fluxes are from the ERA5 reanalysis  
105 by the European Centre for Medium-Range Weather Forecasts (ECMWF) (Hersbach et  
106 al., 2020), which replaces the ERA-Interim reanalysis that ceased production in 2019.  
107 The variables used in this study are monthly downward longwave radiation (DLR), net  
108 longwave radiation (NLR), downward shortwave radiation (DSR), net shortwave  
109 radiation (NSR), surface latent heat flux (SLHF), surface sensible heat flux (SSHF),  
110 total-column water vapor (TWV), and SAT and wind fields at the 850-hPa level, for the  
111 month of May from 1979 to 2018. The spatial resolution of ERA5 used in this study is  
112  $0.25^{\circ} \times 0.25^{\circ}$ , less than 30 km in the region of the Laptev Sea and East Siberian Sea.  
113 Note that the four components of the surface energy balance (SEB) include NLR, NSR,  
114 SLHF, and SSHF.

115

116

### 117 **3. Results**

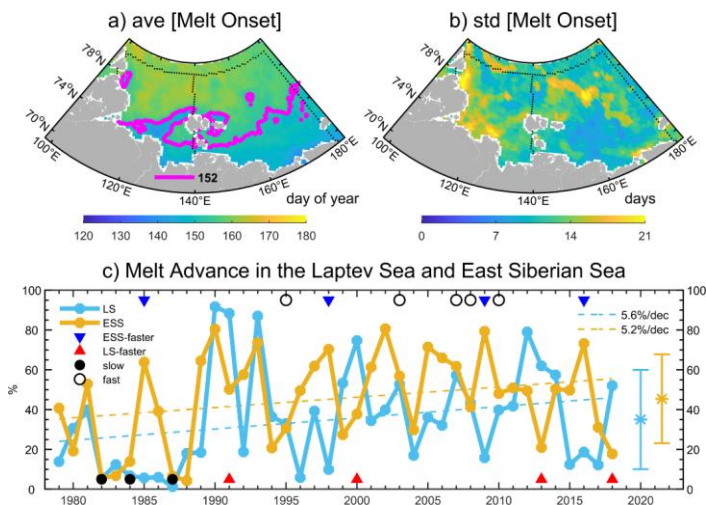
#### 118 *3.1 Distinct Melt Advance Scenarios in the Laptev Sea and East Siberian Sea*

119 Sea ice begins to melt at the surface in spring when solar radiation increases and the  
120 atmosphere warms. On average, the sea ice surface in the Laptev Sea (LS) and East  
121 Siberian Sea (ESS) begins to melt during May and June (Fig. 1a). Naturally, sea ice  
122 melting advances northward in a given year. The range for the interannual change of  
123 MO in a given place is expected to be around one month (Fig. 1b). In order to  
124 demonstrate the progress of MO in different years, melt advance (MA) is defined by  
125 calculating the areal percentage of an individual sea that has experienced MO at the end  
126 of May (see magenta contour line in Fig. 1a). In this way, we can detect whether sea-  
127 ice surface melting advances slowly or quickly in a specific year, as well as the spatial  
128 patterns of the melt advance. For the seasonal prediction of summer sea ice, this metric

129 of Melt Advance is in essence similar to the average MO date, but may have advantages  
 130 if we can get real-time satellite MO for the region. Then, at the end of May or other  
 131 specific date, we can get the MA pattern which supports timely seasonal prediction.

132 Figure 1c shows the time series of MA for the LS and ESS during 1979-2018. The  
 133 variability is large, ranging from near zero to 100%. This implies changeable spring  
 134 conditions on the interannual scale. On average, MA is around 40% for each sea,  
 135 meaning that ~40% of the sea area has experienced sea-ice surface melting at the end  
 136 of May. In the context of global warming, MA has an increasing tendency in both seas  
 137 although this tendency is not quite significant (less than 6% per decade). This indicates  
 138 that we sometimes need to pay more attention to the interannual variability than to the  
 139 long-term linear tendency. We can also notice that relatively slow MA in the 1980s  
 140 contributes considerably to the overall positive tendency.

141



142  
 143 **Fig. 1.** (a, b) Climatology and standard deviation of sea ice Melt Onset, and (c) Melt  
 144 Advance time series in the Laptev Sea and East Siberian Sea, 1979-2018. The magenta  
 145 lines in panel (a) are contours of 152 (day of year), representing the end of May. The  
 146 areal percentage of sea ice Melt Onset earlier than 152 (day of year) is defined as Melt  
 147 Advance. In panel (c), only the trend of Melt Advance in the ESS is statistically  
 148 significant at the 90% confidence level. The average and standard deviation of the Melt  
 149 Advance in the LS and ESS are  $35\% \pm 25\%$  and  $45\% \pm 22\%$ , respectively. Sample years  
 150 (16 out of the long time-series) that fall into one of four categories are marked (see also

151 Table 1).

152

153 Another feature is related to the relationship of MA between the LS and ESS. In  
154 some years, MA in both the LS and ESS is slow, as in the 1980s; in other years, MA in  
155 both seas may be fast; and in other years, MA can be substantially different in the two  
156 seas. Thus, four categories of sample years are selected for further composite analysis  
157 (Table 1 and markers in Fig. 1c; MA difference between the LS and ESS is shown in  
158 Fig. S2), which represent four basic scenarios of MA in this region. Specifically, years  
159 with significantly faster MA in the ESS than in the LS ( $\delta > 48\%$ ) are grouped as the ESS-  
160 faster-scenario, while years with significantly faster MA in the LS than in the ESS  
161 ( $\delta > 33\%$ ) are classified as the LS-faster-scenario. The slow-scenario includes years  
162 when MA in both seas is slow (below 20%), while the fast-scenario consists of years  
163 when MA in both seas is relatively fast (between 30% and 60% at the same time). So,  
164 two pairs of contrasting categories are formed (ESS-faster-scenario vs. LS-faster-  
165 scenario, slow-scenario vs. fast-scenario). Note that to some extent the latter two  
166 scenarios represent the contrast between the 1980s and subsequent decades. Such  
167 categorization also reflects the large variability of MA in spring from the interannual  
168 perspective.

169

Category	Years	Description
ESS-faster-scenario	1985, 1998, 2009, 2016	significantly faster Melt Advance ( $\delta > 48\%$ ) in the ESS than in the LS
LS-faster-scenario	1991, 2000, 2013, 2018	significantly faster Melt Advance ( $\delta > 33\%$ ) in the LS than in the ESS
slow-scenario	1982, 1984, 1987	similar but slow Melt Advance ( $\delta < 8\%$ , but below 20%)
fast-scenario	1995, 2003, 2007, 2008, 2010	similar but fast Melt Advance ( $\delta < 9\%$ , but between 30% and 60%)

170 **Table 1** List of years under different scenarios of Melt Advance.

171 Note: Practically, the ESS-faster-scenario and LS-faster-scenario are selected based on  
172 one standard deviation of the difference in Melt Advance between the Laptev Sea and  
173 East Siberian Sea. The slow-scenario and fast-scenario include years when Melt  
174 Advance in the two seas is quite close. All years listed here are marked in Fig. 1c.

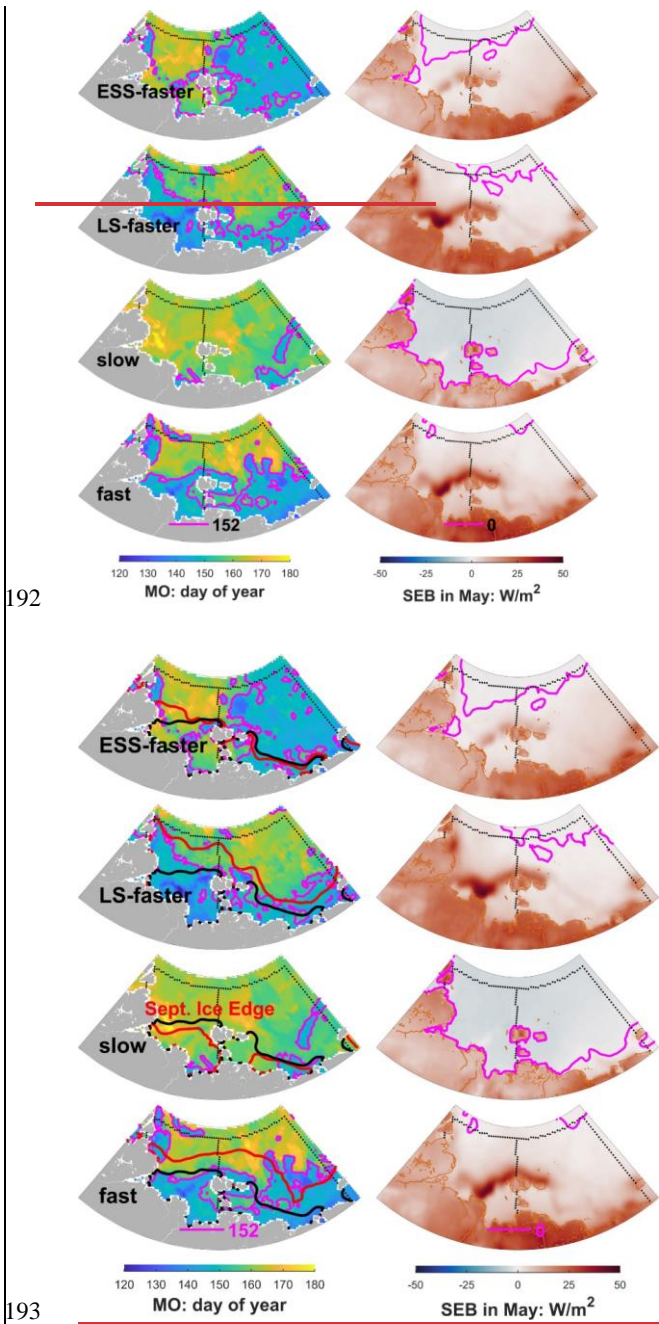
175

176 Composite results show that the ESS-faster-scenario has substantially earlier MO,  
177 i.e., faster MA in the ESS than in the LS, while the LS-faster-scenario has a somewhat  
178 opposite signal (indicated by the magenta line in Fig. 2). For the slow-scenario, little  
179 area in either sea has experienced MO until the end of May, indicating slow MA; for  
180 the fast-scenario, nearly half of both seas has begun to experience sea-ice surface  
181 melting, indicating fast MA at almost the same pace. From the surface energy balance  
182 (SEB) in May, we find consistent patterns. With the zero lines of SEB as a reference,  
183 the ESS-faster-scenario has relatively more positive SEB in the ESS than in the LS,  
184 while the opposite is true for the LS-faster-scenario. For the slow-scenario, SEB is  
185 negative over most of the two seas, while for the fast-scenario, SEB is positive in both  
186 seas. This fits well with common sense. Although MA-related albedo changes may  
187 amplify the SEB signals in a two-way interaction, it is fair to say that SEB in May  
188 drives different patterns of MA (see individual years in Fig. S3).

189 In the next section, we investigate systematic processes under different MA  
190 scenarios that involve the atmosphere, sea ice, and surface energy fluxes.

191





194 **Fig. 2.** Composites of MO and surface energy balance (SEB) in May for the four  
 195 scenarios. The left column shows the MO patterns marked by magenta contour lines

Formatted: Normal (Web)

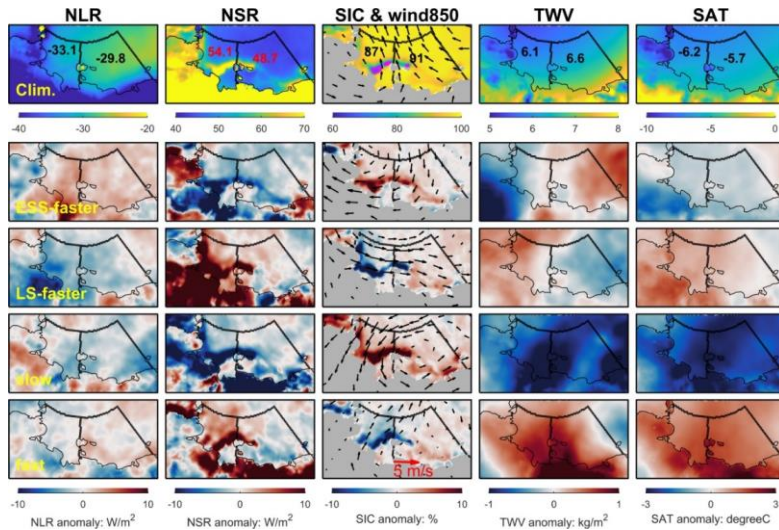
196 with the value of 152 (day of year) which represents the end of May. Red contour lines  
 197 show the composite September ice edge, while black contour lines denote the  
 198 climatological September ice edge for 1979-2018. The right column is the SEB in May,  
 199 with magenta contour lines of zero. Black dots denote the boundaries of the LS and  
 200 ESS.

201

202 *3.2 Dynamic and Thermodynamic Processes under Different Melt Advance Scenarios*

203 Climatologically, SEB is basically positive ( $\sim 5 \text{ W/m}^2$ ) across the two seas in May  
 204 (see first row in Fig. S4). Among the components, it is positive net shortwave radiation  
 205 (NSR) that compensates for losses from net longwave radiation (NLR), SLHF, and  
 206 SSHF. This implies that on average the atmosphere receives energy from the surface  
 207 through the latter three components in May. SAT is around  $-6^\circ\text{C}$ , while sea ice almost  
 208 fully covers the ocean ( $\sim 90\%$ ) (see first row in Fig. 3). In the lower troposphere (850  
 209 hPa), southeasterlies blow across the region, which to some extent explains the  
 210 existence of polynyas in the middle LS, i.e., regions where sea ice concentration is  
 211 below 75%. Note that Fig. 3 shows only selected vital variables; other relevant factors  
 212 can be found in Fig. S4-S7.

213



214 **Fig. 3.** Climatology (first row) and composite anomalies for the four scenarios (lower  
 215 four rows) of relevant atmospheric and sea ice variables in May: NLR, NSR, SIC, winds  
 216

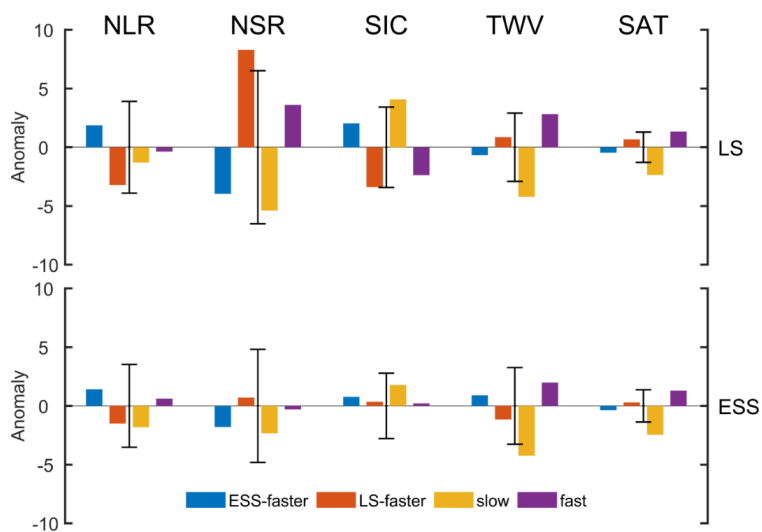
217 at 850 hPa, TWV, and SAT. Numbers within the LS and ESS are the region-mean values,  
218 respectively. Note that magenta lines in the climatological SIC fields denote contours  
219 of 75% SIC values, which suggest the location of polynyas.

220

221 In the ESS-faster-scenario (see second row in Fig. 3 and blue bars in Fig. 4),  
222 prevailing northeasterlies in the lower troposphere tend to increase SIC and reduce  
223 polynya area, especially for the LS, which increases surface albedo and decreases solar  
224 radiation absorption. The northeasterlies seem to also bring slightly cool air masses to  
225 the region, and slightly moist air masses to the ESS. Given that sea ice cover is more  
226 packed, longwave radiation loss from the surface to the atmosphere is reduced, which  
227 to some extent compensates for the reduced solar radiation absorption. Due to the  
228 greater negative anomaly of solar radiation absorption in the LS, the net surface energy  
229 balance is a loss in the LS, but a gain in the ESS (Fig. S4 and S6). In addition, sea-ice  
230 surface melting is usually preconditioned by increased water vapor in the atmosphere  
231 (Mortin et al., 2016). So, faster Melt Advance in the ESS is expected as TWV is  
232 increased in the ESS. However, in this case, as depicted in Fig. 4, no anomaly extends  
233 beyond the interannual standard deviation for the LS and ESS, suggesting a risk of over-  
234 interpretation. One plausible explanation is that the normal state in this region tends to  
235 resemble the ESS-faster-scenario, as indicated by Fig. 1a and the higher climatological  
236 Melt Advance value in the ESS compared to the LS shown in Fig. 1c. Additionally,  
237 multiple atmospheric setups may lead to the ESS-faster-scenario, highlighting the  
238 considerable variability in springtime conditions. Hence, the low signal-to-noise ratio  
239 is understandable. It's worth noting that the LS exhibits more notable differences,  
240 consistent with its significant polynya activity.

241 For the LS-faster-scenario (see third row in Fig. 3 and red bars in Fig. 4), wind fields  
242 at 850-hPa show unified westerlies over the LS and northwesterlies over the ESS, which  
243 to some extent account for the reduced sea ice cover in the LS and the slightly packed  
244 sea ice in the ESS. While the westerlies may not fully account for the reduced sea ice  
245 in the LS, this ~~Such~~ circulation ~~has~~ includes an offshore wind component in the western

246 ~~LS, resulting in increased and drive sea ice out of the LS, which probably leads to more~~  
 247 ~~polynya opening. This includes polynyas such as the Northeast Taymyr polynya, the~~  
 248 ~~Taymyr polynya, and the Anabar-Lena polynya –and reduced SIC~~ (Krumpen et al.,  
 249 2011). So, we see a substantial increase in solar radiation absorption (beyond one  
 250 standard deviation) in the LS. While longwave radiation loss is somehow enhanced, the  
 251 net surface energy balance is still a gain for the LS and a loss for the ESS. The westerlies  
 252 may also bring warm and wet air masses from the North Atlantic and contribute to  
 253 positive anomalies of TWV and SAT in the LS, which promotes faster MA. We may  
 254 expect that reduced sea ice cover in the LS enables more moisture to be released from  
 255 the exposed ocean. However, latent heat loss as well as sensible heat loss toward  
 256 atmosphere in the LS weakens (Fig. S4 and S6), which suggests that warmer and  
 257 moister atmosphere is mainly a result of air mass transport and in turn reduces turbulent  
 258 heat loss from the surface.  
 259



260  
 261 **Fig. 4.** Region-mean composite anomalies in the LS and ESS for the four scenarios  
 262 shown in Fig. 3. The error bars denote the corresponding standard deviation for 1979-  
 263 2018. The variables of NLR, NSR, SIC, TWV, and SAT have units of  $W/m^2$ ,  $W/m^2$ , %,   
 264  $kg/m^2$ , and K, respectively. Here, SIC is represented by the areal percentage of sea ice  
 265 cover relative to the whole sea. To facilitate viewing, TWV is scaled by a factor of 5.  
 266

267 For the slow-scenario (see fourth row in Fig. 3, and orange bars in Fig. 4), a cyclonic  
268 anomaly in the lower troposphere, which is centered on the ESS, pushes sea ice against  
269 the southern coast in the western half of the LS, and against the fast ice zone in the  
270 eastern half, thereby preventing polynya formation. More sea ice cover in both seas  
271 decreases solar radiation absorption. Meanwhile, this region is under the influence of  
272 cold and dry air masses (beyond one standard deviation), which induce a large loss of  
273 longwave radiation and SSHF from the surface. As a whole, we see unified surface  
274 energy deficits in the LS and ESS (beyond one standard deviation). Note that all the  
275 three sample years are from the 1980s. So, the larger sea ice cover and cooler  
276 atmosphere mainly reflect the Arctic state in the 1980s, which is a decadal phenomenon  
277 rather than interannual characteristics. We also examine the monthly snowfall under the  
278 four scenarios (Fig. S5). For this region, snowfall dominates the total precipitation in  
279 May. Especially for the slow melt advance scenario, snowfall is abnormally high, which  
280 will also result in high surface albedo.

281 For the fast-scenario, with sample years after the 1980s (see last row in Fig. 3, and  
282 purple bars in Fig. 4), southerlies in the lower troposphere blow mainly across the LS,  
283 which drive sea ice off the coast, open the polynya and in turn increase shortwave  
284 radiation absorption. At the same time, the southerlies bring warm and wet air masses  
285 to this region, which substantially reduce the SSHF loss from the surface. As a result,  
286 we see a positive net surface energy balance in this region and relatively fast MA.

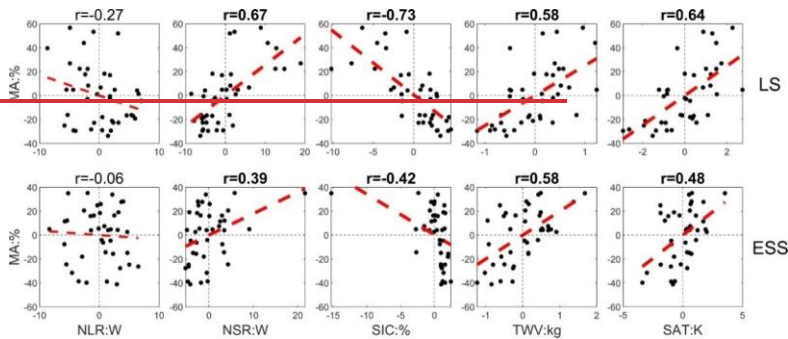
287 The composite analysis above indicates that circulation in the lower troposphere in  
288 spring in this region can be quite changeable (see individual years in Fig. S8), which  
289 can have two effects: one is related to sea ice dynamics; the other involves moisture  
290 and air mass advection. The former produces strong regulation of NSR due to albedo  
291 changes, while the latter has everything to do with the atmospheric state, which favors  
292 sea-ice surface melting when the atmosphere is warm and wet.

293 Figure 5 further shows the statistical correlation related to MA, covering years from  
294 1979 to 2018. In general, we see that faster MA is accompanied by warm and wet

295 atmosphere. The related atmospheric circulation in the lower troposphere may also  
296 drive reduced SIC and subsequent increased solar radiation absorption. Note that the  
297 variability of SIC and NSR in the ESS is smaller than in the LS if the single outlier is  
298 removed from the ESS data (see the second and third plots in the bottom row of Fig. 5).  
299 Once more, this is related to the significant polynya activity observed in the LS. In  
300 addition, Mortin et al. (2016) argued that on a synoptic scale, increased water vapor in  
301 the atmosphere favors stronger DLR, which promotes sea-ice surface melting. Such  
302 conclusion makes sense when we focus on sea ice and atmosphere above. While we  
303 examine from the perspective of the whole region, including effects of the open ocean,  
304 results here suggest that on the subseasonal scale net longwave radiation has little  
305 connection with MA (see first column in Fig. 5). To some extent, the weak correlation  
306 even shows that on the monthly scale, longwave radiation loss tends to be more when  
307 SEB is more and MA is faster, which suggests some negative feedback probably related  
308 to the open ocean.

309 While NSR is strong, downward shortwave radiation tends to be less (see Fig. S9),  
310 which is expected from more moisture in the atmosphere. However, cloud analysis  
311 based on ERA5 reanalysis doesn't suggest significant effects of clouds. Total cloud  
312 cover in this region generally is larger than 90% in May and interannual anomaly is  
313 relatively small (less than 5%, see Fig. S5). This indicates that from the perspective of  
314 anomaly, water vapor rather than cloud cover has considerable radiation effects in the  
315 springtime. Given the large uncertainty of clouds in current datasets, this remains an  
316 open question.

317



Formatted: Space Before: Auto, After: Auto

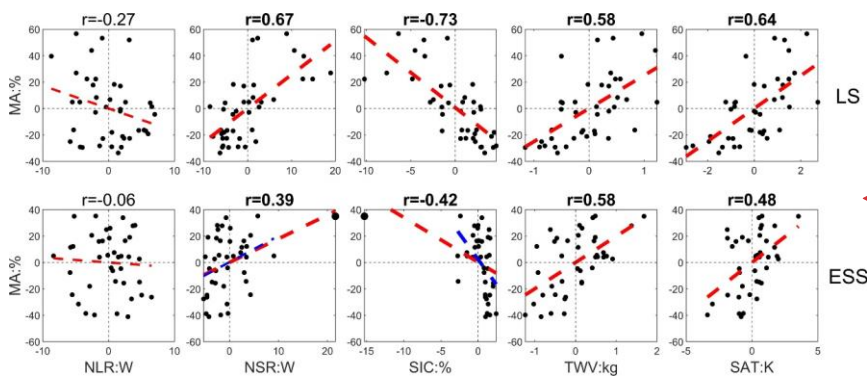


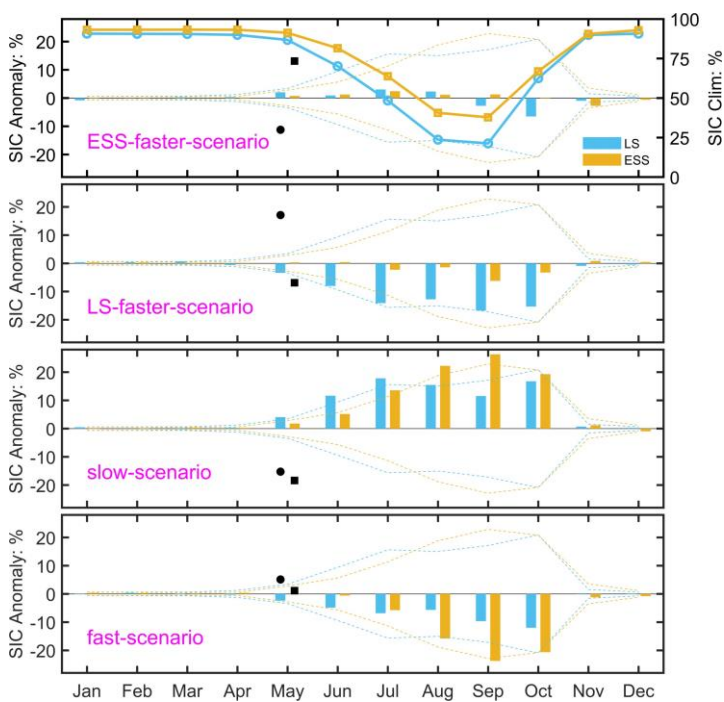
**Fig. 5.** Scatter plots for the period 1979-2018, illustrating the relationship between the Melt Advance (MA) anomaly and region-mean anomalies of factors shown in Figs. 3 and 4. Thick dashed red lines denote represent linear fits above the 95% confidence level. Bold titles represent correlation above the 95% confidence level. In the second and third plots of the bottom row, thin and thick dashed blue lines respectively denote linear fits after the removal of an outlier, identified by a larger black dot.

To what extent do different sea-ice surface melting scenarios in spring have implications for sea ice cover in summer? Could we gain seasonal prediction skill based on detection of sea-ice surface melting in spring? For the selected Melt Advance scenarios, sea ice cover in September somewhat responds accordingly (see left column in Fig. 2). In the ESS-faster-scenario, sea ice edge in September is close to climatology. This echoes that the ESS-faster-scenario reflects the climatology of Melt Advance, too (Fig. 1a). In the LS-faster-scenario, sea ice edge in September retreats more northward



334 in the LS part. In the slow-scenario, sea ice edge is nearer the southern coast; while in  
 335 the fast-scenario, sea ice edge retreats considerably in both seas. The results above  
 336 suggest that sea ice edge in September tends to be northward if Melt Advance at the  
 337 end of May is fast. Further investigation of seasonal transition of sea ice cover in the  
 338 four Melt Advance scenario indicates similar relationship (Fig. 6).

339



340

341 Fig. 6. Annual cycle of SIC anomaly in the four scenarios of Melt Advance. SIC is  
 342 denoted by the areal percentage of sea ice cover relative to the whole sea. Dotted lines  
 343 are the standard deviation. The mean Melt Advance in the LS and ESS is also marked  
 344 by solid dots and squares.

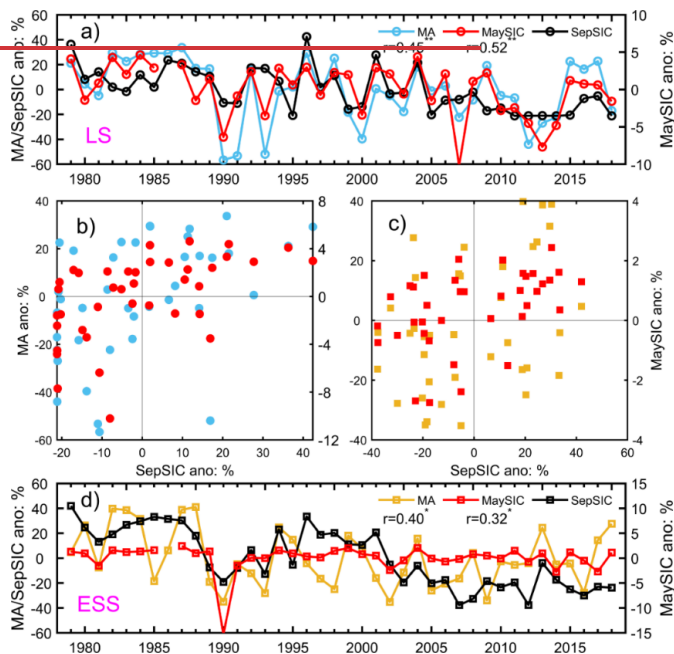
345

346 ~~A simple way to address this is to put aside the processes linking spring and summer~~  
 347 ~~and directly investigate the statistical relationship between sea ice surface melting~~  
 348 ~~scenarios in spring and sea ice states in summer.~~ Figure 6 shows that in both the LS and  
 349 ESS, Melt Advance in spring is significantly correlated with sea ice cover in September,  
 350 which is consistent with previous studies utilizing Melt Onset as a predictor of summer

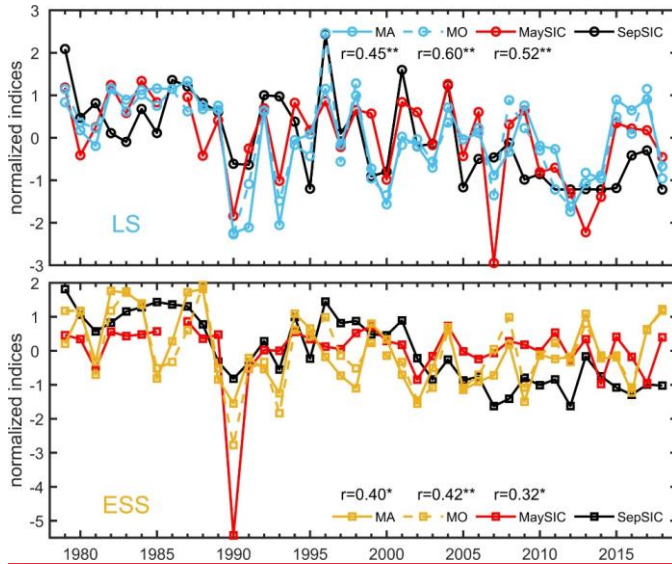


351 sea ice (Petty et al., 2017; Wang et al., 2011). ~~However~~ Besides, it has ~~no stronger~~ similar  
 352 prediction skill (statistical correlation) as average MO or than SIC in May. In general,  
 353 ~~the connection between springtime and summer seems to be stronger in the LS than in~~  
 354 ~~the ESS. Given that the metric of Melt Advance can be reliably defined on the same~~  
 355 ~~day every year (not necessarily the end of May), it has the potential to be fed into the~~  
 356 ~~statistical or Artificial Intelligence prediction of summer sea ice cover once real-time~~  
 357 ~~satellite detection is available. At least, it can be commonly used as the average Melt~~  
 358 ~~Onset, it seems that MA performs slightly better than May SIC predicting the~~  
 359 ~~September SIC. The main reason may be that May SIC in the ESS has small interannual~~  
 360 ~~variability, which is consistent with the lack of polynya activity in the ESS relative to~~  
 361 ~~the LS. Beyond this, for the prediction of summer sea ice cover, the seasonal evolution~~  
 362 ~~from spring to summer is still a challenge as it is not fully understood. Processes during~~  
 363 ~~the melting season may strongly disturb the signal from the Melt Advance (Fig. S10).~~  
 364 ~~More study of seasonal evolution in the Arctic is needed in the future.~~

365



366



Formatted: Normal (Web), Line spacing: single

367

368 **Fig. 67.** Sea-ice surface Melt Advance, average Melt Onset, and Sea Ice Concentration  
 369 (SIC) in May and September sea-ice cover in the Laptev Sea (subplot a and b top) and  
 370 East Siberian Sea (subplot c and d bottom),) from 1979- to 2018. The May and  
 371 September sea ice cover is are denoted by the areal percentage of sea-ice cover relative  
 372 to the whole sea. All variables have been normalized. To facilitate viewing For better  
 373 visualization, Melt Advance is timed-multiplied by -1. Correlation coefficients with  
 374 double asterisks denote 99% confidence, while those with a single asterisk denote 90%  
 375 confidence.

376

377

378

#### 379 4. Discussion

380 In this study, sampling for different scenarios of sea ice Melt Advance is based on  
 381 the Melt Onset dataset, which is a satellite observation product. To our knowledge,  
 382 ERA5 to some extent incorporates the sea ice concentration dataset of OSI SAF, but  
 383 not the Melt Onset dataset (Hersbach et al., 2020). ERA5 atmospheric reanalysis and  
 384 different Melt Advance patterns can be seen as independent sources of information and  
 385 their consistency should provide more confidence.

386 In fact, the concept of Melt Advance can be used for the whole Arctic, and can

387 describe how sea-ice surface melting advances in spring. As mentioned above, Melt  
388 Advance can also be used as relatively independent information with reference to an  
389 atmospheric reanalysis dataset. Liang and Zhou (2023) identified three modes of Melt  
390 Onset in the LS and ESS by EOF decomposition. The positive L-mode and E-mode in  
391 their study correspond to LS-faster-scenario and ESS-faster-scenario, while the positive  
392 and negative LE-mode relate to fast-scenario and slow-scenario, respectively.

393 Regarding SIC anomaly in the LS and ESS, we should bear in mind that before  
394 melting the shelf areas of the LS and ESS are covered with extensive fast ice (up to 200  
395 km wide), which is formed by April (Selyuzhenok et al., 2015). SIC in May can increase  
396 due to specific wind fields, but it probably does not consolidate against the land. Instead,  
397 the SIC anomaly is closely related to polynya development. As Fig. 3 shows, the largest  
398 SIC anomaly under the four scenarios usually occurs around the polynya region  
399 (Willmes et al., 2011).

400

401

## 402 **5. Conclusions**

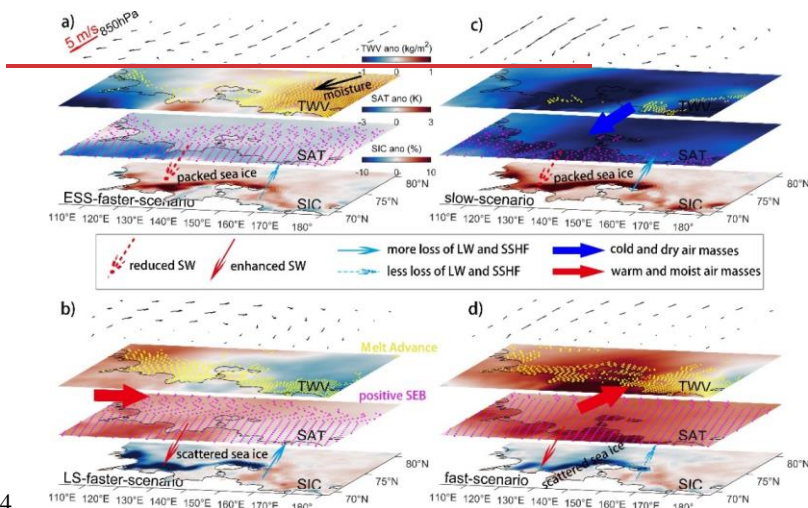
403 In this study, the metric of Melt Advance (MA) is used to measure sea-ice surface  
404 melting instead of region-mean Melt Onset. MA is defined as the areal percentage of a  
405 sea in which the sea ice surface has begun to melt at the end of May, in this case the  
406 Laptev Sea (LS) and East Siberian Sea (ESS). This metric has the potential to help  
407 seasonally predict summer sea ice for the whole Arctic.

408 Four representative scenarios of Melt Advance in the LS and ESS are identified: the  
409 ESS-faster-scenario, LS-faster-scenario, slow-scenario, and fast-scenario. Composite  
410 analyses reveal that in these distinct scenarios of Melt Advance, atmospheric circulation,  
411 sea ice dynamics (polynya activities), air mass advection, and surface energy fluxes are  
412 related with each other. -ESS-faster-scenario is associated with positive TWV anomaly  
413 over the ESS and negative TWV anomaly over the LS. LS-faster-scenario and fast-  
414 scenario seem to occur when polynya in the Laptev Sea opens. But the slow-scenario

415 mainly reflect the cool Arctic state in the 1980s. In addition, polynya activity in this  
 416 region and initial sea ice condition are also not neglectable. ~~The main conclusions are~~  
 417 ~~demonstrated in the schematic of Fig. 7.~~

418 Although sea ice Melt Advance as well as average Melt Onset and –sea ice cover  
 419 in May are both statistically correlated with sea ice cover in September, seasonal  
 420 evolution can to a large extent disturb this linkage. This study suggests a need to further  
 421 investigate the changeable spring circulation in the lower troposphere and seasonal  
 422 evolution in the Arctic.

423



424 **Fig. 7. Schematic processes under the four scenarios of sea ice Melt Advance in the LS**  
 425 **and ESS. a) ESS-faster-scenario; b) LS faster-scenario; c) slow-scenario; d) fast-**  
 426 **scenario. For each scenario, four layers represent composite anomalies of wind fields**  
 427 **at 850 hPa, TWV, SAT, and SIC, respectively. Thin arrows denote shortwave radiation**  
 428 **(red), and longwave radiation and sensible heat flux (cyan), while solid and dashed**  
 429 **types suggest the fluxes enhanced or weakened. Bold blue arrow refers to transport of**  
 430 **cold and dry air masses, while bold red arrow refers to warm and moist advection.**  
 431 **Yellow dots superimposed upon TWV show Melt Advance by the end of May. Magenta**  
 432 **dots upon SAT denote positive surface energy balance (SEB).**

434 *Data Availability Statement.*

435 The sea ice MO dataset is from NASA's Cryospheric Sciences Research Portal  
436 (<https://earth.gsfc.nasa.gov/cryo/data/arctic-sea-ice-melt>). SAT of IABP/POLES can be  
437 accessed at <https://arcticdata.io/catalog/view/doi:10.18739/A2J598>, and SAT of AIRS  
438 at [https://disc.gsfc.nasa.gov/datasets/AIRS3STD\\_006/summary](https://disc.gsfc.nasa.gov/datasets/AIRS3STD_006/summary). The SIC dataset of  
439 OSI SAF was downloaded from the websites below:  
440 <ftp://osisaf.met.no/reprocessed/ice/conc/v2p0/> and  
441 <ftp://osisaf.met.no/reprocessed/ice/conc-cont-reproc/v2p0/>.  
442 The ERA5 reanalysis dataset was retrieved at  
443 [https://cds.climate.copernicus.eu/cdsapp#!/search?type=dataset&keywords=\(\(%20%20%20Product%20type:%20Reanalysis%22%20\)\)](https://cds.climate.copernicus.eu/cdsapp#!/search?type=dataset&keywords=((%20%20%20Product%20type:%20Reanalysis%22%20))). In this study, we used ERA5 monthly  
444 averaged data at single level and pressure levels.  
445

446

447 *Author Contribution*

448 Hongjie Liang [Formal analysis; Writing original draft].

449 Wen Zhou [Funding acquisition; Supervision].

450

451 *Competing interests*

452 The authors declare that they have no conflict of interest.

453

454 *Acknowledgments.*

455 This work was supported by the National Natural Science Foundation of China (Grant  
456 No. 42288101, 42120104001).

457

458

459 REFERENCES

- 460 Bliss, A. and Anderson, M.: Snowmelt onset over Arctic sea ice from passive  
461 microwave satellite data: 1979–2012, *The Cryosphere*, 8, 2089–2100, 10.5194/tc-  
462 8-2089-2014, 2014.
- 463 Budyko, M. I.: The effect of solar radiation variations on the climate of the Earth, *Tellus*,  
464 21, 611–619, 10.1111/j.2153-3490.1969.tb00466.x, 1969.
- 465 Cavalieri, D., Parkinson, C., Gloersen, P., and Zwally, H.: Sea ice concentrations from  
466 Nimbus-7 SMMR and DMSP SSM/I passive microwave data, National Snow and  
467 Ice Data Center, Boulder, Colorado, USA, 10.5067/8GQ8LZQVL0VL, 1996.
- 468 Cohen, J., Screen, J. A., Furtado, J. C., Barlow, M., Whittleston, D., Coumou, D.,

469 Francis, J., Dethloff, K., Entekhabi, D., Overland, J., and Jones, J.: Recent Arctic  
470 amplification and extreme mid-latitude weather, *Nature Geoscience*, 7, 627-637,  
471 10.1038/ngeo2234, 2014.

472 Crawford, A. D., Horvath, S., Stroeve, J., Balaji, R., and Serreze, M. C.: Modulation of  
473 Sea Ice Melt Onset and Retreat in the Laptev Sea by the Timing of Snow Retreat  
474 in the West Siberian Plain, *Journal of Geophysical Research: Atmospheres*, 123,  
475 8691-8707, 10.1029/2018jd028697, 2018.

476 Drobot, S. D. and Anderson, M. R.: An improved method for determining snowmelt  
477 onset dates over Arctic sea ice using scanning multichannel microwave radiometer  
478 and Special Sensor Microwave/Imager data, *Journal of Geophysical Research:*  
479 *Atmospheres*, 106, 24033-24049, 10.1029/2000JD000171, 2001.

480 Francis, J. A. and Vavrus, S. J.: Evidence for a wavier jet stream in response to rapid  
481 Arctic warming, *Environmental Research Letters*, 10, 10.1088/1748-  
482 9326/10/1/014005, 2015.

483 Hersbach, H., Bell, B., Berrisford, P., Hirahara, S., Horányi, A., Muñoz - Sabater, J.,  
484 Nicolas, J., Peubey, C., Radu, R., Schepers, D., Simmons, A., Soci, C., Abdalla,  
485 S., Abellan, X., Balsamo, G., Bechtold, P., Biavati, G., Bidlot, J., Bonavita, M.,  
486 Chiara, G., Dahlgren, P., Dee, D., Diamantakis, M., Dragani, R., Flemming, J.,  
487 Forbes, R., Fuentes, M., Geer, A., Haimberger, L., Healy, S., Hogan, R. J., Hólm,  
488 E., Janisková, M., Keeley, S., Laloyaux, P., Lopez, P., Lupu, C., Radnoti, G.,  
489 Rosnay, P., Rozum, I., Vamborg, F., Villaume, S., and Thépaut, J. N.: The ERA5  
490 global reanalysis, *Quarterly Journal of the Royal Meteorological Society*, 146,  
491 1999-2049, 10.1002/qj.3803, 2020.

492 Horvath, S., Stroeve, J., Rajagopalan, B., and Jahn, A.: Arctic sea ice melt onset favored  
493 by an atmospheric pressure pattern reminiscent of the North American-Eurasian  
494 Arctic pattern, *Climate Dynamics*, 57, 1771-1787, 10.1007/s00382-021-05776-y,  
495 2021.

496 Kashiwase, H., Ohshima, K. I., Nihashi, S., and Eicken, H.: Evidence for ice-ocean  
497 albedo feedback in the Arctic Ocean shifting to a seasonal ice zone, *Sci Rep*, 7,  
498 8170, 10.1038/s41598-017-08467-z, 2017.

499 Krumpfen, T., Hölemann, J. A., Willmes, S., Morales Maqueda, M. A., Busche, T.,  
500 Dmitrenko, I. A., Gerdes, R., Haas, C., Heinemann, G., Hendricks, S., Kassens,  
501 H., Rabenstein, L., and Schröder, D.: Sea ice production and water mass  
502 modification in the eastern Laptev Sea, *Journal of Geophysical Research*, 116,  
503 10.1029/2010jc006545, 2011.

504 Lavergne, T., Sørensen, A. M., Kern, S., Tonboe, R., Notz, D., Aaboe, S., Bell, L.,  
505 Dybkjær, G., Eastwood, S., Gabarro, C., Heygster, G., Killie, M. A., Brandt  
506 Kreiner, M., Lavelle, J., Saldo, R., Sandven, S., and Pedersen, L. T.: Version 2 of  
507 the EUMETSAT OSI SAF and ESA CCI sea-ice concentration climate data  
508 records, *The Cryosphere*, 13, 49-78, 10.5194/tc-13-49-2019, 2019.

509 Lei, R., Cheng, B., Hoppmann, M., Zhang, F., Zuo, G., Hutchings, J. K., Lin, L., Lan,  
510 M., Wang, H., Regnery, J., Krumpfen, T., Haapala, J., Rabe, B., Perovich, D. K.,

511 and Nicolaus, M.: Seasonality and timing of sea ice mass balance and heat fluxes  
512 in the Arctic transpolar drift during 2019–2020, *Elementa: Science of the*  
513 *Anthropocene*, 10, 10.1525/elementa.2021.000089, 2022.

514 Liang, H. and Su, J.: Variability in Sea Ice Melt Onset in the Arctic Northeast Passage:  
515 Seesaw of the Laptev Sea and the East Siberian Sea, *Journal of Geophysical*  
516 *Research: Oceans*, 126, e2020JC016985, 10.1029/2020JC016985, 2021.

517 Liang, H. and Zhou, W.: Arctic Sea Ice Melt Onset in the Laptev Sea and East Siberian  
518 Sea in Association with the Arctic Oscillation and Barents Oscillation, *Journal of*  
519 *Climate*, 36, 6363–6373, 10.1175/jcli-d-22-0791.1, 2023.

520 Markus, T., Stroeve, J. C., and Miller, J.: Recent changes in Arctic sea ice melt onset,  
521 freezeup, and melt season length, *Journal of Geophysical Research (Oceans)*, 114,  
522 C12024, 10.1029/2009jc005436, 2009.

523 Mortin, J., Svensson, G., Graverson, R. G., Kapsch, M.-L., Stroeve, J. C., and Boisvert,  
524 L. N.: Melt onset over Arctic sea ice controlled by atmospheric moisture transport,  
525 *Geophysical Research Letters*, 43, 6636–6642, 10.1002/2016GL069330, 2016.

526 Petty, A. A., Kurtz, N. T., Kwok, R., Markus, T., and Neumann, T. A.: Winter Arctic Sea  
527 Ice Thickness From ICESat - 2 Freeboards, *Journal of Geophysical Research:*  
528 *Oceans*, 125, 10.1029/2019jc015764, 2020.

529 Petty, A. A., Schröder, D., Stroeve, J. C., Markus, T., Miller, J., Kurtz, N. T., Feltham,  
530 D. L., and Flocco, D.: Skillful spring forecasts of September Arctic sea ice extent  
531 using passive microwave sea ice observations, *Earth's Future*, 5, 254–263,  
532 10.1002/2016ef000495, 2017.

533 Screen, J. A. and Simmonds, I.: The central role of diminishing sea ice in recent Arctic  
534 temperature amplification, *Nature*, 464, 1334–1337, 10.1038/nature09051, 2010.

535 Sellers, W. D.: A Global Climatic Model Based on the Energy Balance of the Earth-  
536 Atmosphere System, *Journal of Applied Meteorology and Climatology*, 8, 392-  
537 400, 10.1175/1520-0450(1969)008<0392:agcmbo>2.0.co;2, 1969.

538 Selyuzhenok, V., Krumpfen, T., Mahoney, A., Janout, M., and Gerdes, R.: Seasonal and  
539 interannual variability of fast ice extent in the southeastern Laptev Sea between  
540 1999 and 2013, *Journal of Geophysical Research: Oceans*, 120, 7791–7806,  
541 10.1002/2015jc011135, 2015.

542 Serreze, M. C., Barrett, A. P., Stroeve, J. C., Kindig, D. N., and Holland, M. M.: The  
543 emergence of surface-based Arctic amplification, *The Cryosphere*, 3, 11–19,  
544 10.5194/tc-3-11-2009, 2009.

545 Skeie, P.: Meridional flow variability over the Nordic Seas in the Arctic oscillation  
546 framework, *Geophysical Research Letters*, 27, 2569–2572, 10.1029/2000gl011529,  
547 2000.

548 Stroeve, J. and Notz, D.: Changing state of Arctic sea ice across all seasons,  
549 *Environmental Research Letters*, 13, 103001, 10.1088/1748-9326/aade56, 2018.

550 Stroeve, J. C., Markus, T., Boisvert, L., Miller, J., and Barrett, A.: Changes in Arctic  
551 melt season and implications for sea ice loss, *Geophysical Research Letters*, 41,  
552 1216–1225, 10.1002/2013gl058951, 2014.

553 Taylor, P. C., Boeke, R. C., Boisvert, L. N., Feldl, N., Henry, M., Huang, Y., Langen, P.  
554 L., Liu, W., Pithan, F., Sejas, S. A., and Tan, I.: Process Drivers, Inter-Model  
555 Spread, and the Path Forward: A Review of Amplified Arctic Warming, *Frontiers*  
556 *in Earth Science*, 9, 10.3389/feart.2021.758361, 2022.

557 Wang, L., Wolken, G. J., Sharp, M. J., Howell, S. E. L., Derksen, C., Brown, R. D.,  
558 Markus, T., and Cole, J.: Integrated pan-Arctic melt onset detection from satellite  
559 active and passive microwave measurements, 2000-2009, *Journal of Geophysical*  
560 *Research: Atmospheres*, 116, 10.1029/2011jd016256, 2011.

561 Willmes, S., Adams, S., Schröder, D., and Heinemann, G.: Spatio-temporal variability  
562 of polynya dynamics and ice production in the Laptev Sea between the winters of  
563 1979/80 and 2007/08, *Polar Research*, 30, 10.3402/polar.v30i0.5971, 2011.

564